Localization, splitting, and mixing of field emission resonances induced by alkali metal clusters on Cu(100)

S. Stepanow,[1] A. Mugarza,[1] G. Ceballos,[1] and P. Gambardella[1,2]
[1]*Centre d'Investigaciò en Nanociència i Nanotecnologia (ICN-CSIC), UAB Campus, E-08193 Bellaterra, Spain*
[2]*Institució Catalana de Recerca i Estudis Avancats (ICREA), E-08193 Barcelona, Spain*

I. Aldazabal,[3,4] A. G. Borisov,[5] and A. Arnau[3,4]
[3]*Donostia International Physics Center (DIPC), P. de Manuel Lardizabal 4, 20080 San Sebastián/Donostia, Spain*
[4]*Dpto. de Física de Materiales and Centro Mixto CSIC-UPV/EHU, Facultad de Ciencias Químicas, Universidad del País Vasco UPV/EHU, Apto. 1072, 20080 San Sebastián/Donostia, Spain*
[5]*Institut des Sciences Moléculaires d'Orsay, UMR 8214 CNRS-Université Paris–Sud, Bâtiment 351, Université Paris–Sud, 91405 Orsay Cedex, France*

(Received 5 November 2010; published 2 March 2011)

We report on a joint scanning tunneling microscopy (STM) and theoretical wave packet propagation study of field emission resonances (FER's) of nanosized alkali metal clusters deposited on a Cu(100) surface. In addition to FER's of the pristine Cu(100) surface, we observe the appearance of island-induced resonances that are particularly well resolved for STM bias voltage values corresponding to electron energies inside the projected band gap of the substrate. The corresponding dI/dV maps reveal island-induced resonances of different nature. Their electronic densities are localized either inside the alkali cluster or on its boundaries. Our model calculations allow us to explain the experimental results as due to the coexistence and mixing of two kinds of island-induced states. On the one side, since the alkali work function is lower than that of the substrate, the nanosized alkali metal clusters introduce intrinsic localized electronic states pinned to the vacuum level above the cluster. These states can be seen as the FER's of the complete alkali overlayer quantized by the cluster boundaries. On the other side, the attractive potential well due to the alkali metal cluster leads to two-dimensional (2D) localization of the FER's of the Cu(100) surface, the corresponding split component of the resonances appearing below the bottom of the parent continuum. Our main conclusions are based on the attractive nature of the alkali ad-island potential. They are of general validity and, therefore, significant to understand electron confinement in 2D.

DOI: 10.1103/PhysRevB.83.115101 PACS number(s): 73.20.At, 73.20.Hb, 73.22.Dj, 68.37.Ef

I. INTRODUCTION

Scanning tunneling spectroscopy (STS) can be used to investigate unoccupied states at surfaces well above the Fermi level. In the field emission regime, the applied bias is larger than the surface work function and these unoccupied states are strongly distorted by the applied electric field. In this way, image potential states (IS's) are Stark-shifted and actually become field emission resonances (FER's) as observed on different metal[1] and semiconductor surfaces.[2] FER's can be used to chemically identify different surface terminations from a study of the local changes in the work function[3–7] as well as to probe the effects of electron confinement in metallic[8,9] and molecular[10] nanostructures. Since the energetics of FER's is to a large extent determined by the electric field at the junction, the interpretation of the data is relatively simple. This can be done using one-dimensional models,[11,12] as long as both the tip radius of curvature and the lateral extension of the surface area of interest are large compared to the tip-surface distances (a few nanometers when operating the STM at high bias voltages).

However, when the size of the nanostructures on the surface is not too large, the lateral confinement gives rise to a series of nanostructure-localized resonances.[13,14] *A priori*, these are also modified by the electric field. In this case, the interpretation of dI/dV maps and point spectra requires the use of three-dimensional models that explicitly include the applied field. In this work, we present high-resolution low-temperature STS data of alkali (Li) nanoislands grown on Cu(100), as well as model calculations explaining the observed trends in both point spectra and dI/dV maps.

We find that the presence of the alkali clusters of nm size (nanoislands) on the metal surface induces (i) new types of resonances with different azimuthal symmetry (m quantum number)[15,16] that originate from the island-localized image-potential-like states pinned (for low quantum numbers) to the local vacuum level above the island, and (ii) the splitting of the original FER's spatially extended all over the metal surface. Depending on their spatial distribution and relative energy positions, the island-localized resonances can mix with the localized split component of the conventional FER's of the supporting metal surface giving rise to multiple structures observed in dI/dV maps and spectra.

This paper is organized as follows. Section II contains a brief explanation of the experimental system and, as a main result, the STS data including both dI/dV maps and spectra of Li clusters on Cu(100). Section III presents the theoretical approach based on the wave-packet propagation method, a discussion of the relevant approximations, and the interpretation of the experimental data. Finally, Sec. IV reports a summary of the most relevant findings and general conclusions.

II. EXPERIMENT

A. Methods

The experiments were carried out with a low-temperature scanning tunneling microscope (STM) (Createc) under ultrahigh-vacuum conditions. The STM chamber is equipped with standard tools for surface preparation and a combined low-energy-electron-diffraction–Auger system to check the surface cleanliness. The base pressure is better than 2×10^{-10} mbar during preparation and lower than 1×10^{-11} mbar in the STM. The Cu(100) substrate was cleaned by repeated cycles of Ar^+ ion sputtering and annealing to 750 K. Lithium atoms were deposited onto the clean Cu(100) surface held at 300 K using a Li getter source (SAES Getters). The substrate was subsequently transferred to the low-temperature STM and cooled to 5 K.

We focus our investigation on small Li clusters of apparent diameter of about 1.1 nm and height of about 180 pm, when imaged at standard bias and current conditions (0.8 V, 0.3 nA), as shown in Fig. 1. These small clusters are mobile at room temperature, immobile at 5 K, and stable under imaging and spectroscopy conditions. The comparison with manipulation experiments of isolated Li atoms suggests that clusters of this size consist of four to five Li atoms. However, the actual chemical composition of the clusters remains unknown, as it is possible for Cu atoms to intercalate with Li adatoms and form Li-Cu alloy superstructures.[17,18] Experimentally, it was not possible to obtain atomic resolution within the Li clusters.

Field emission resonances (FER's) were investigated by taking differential conductance (dI/dV) spectra in constant current mode (feedback loop closed). At the same time, the relative tip-sample displacement $z(V)$ was recorded. The dI/dV spectra were obtained using a lock-in amplifier modulating the bias voltage at a frequency of 2.5 kHz above the cutoff frequency of the feedback loop with an amplitude V_{rms}=14 mV. The typical acquisition time for a single spectrum is about 10 s. To obtain information on the lateral extension of the resonances, dI/dV maps at a fixed bias voltage were acquired in the constant current mode.

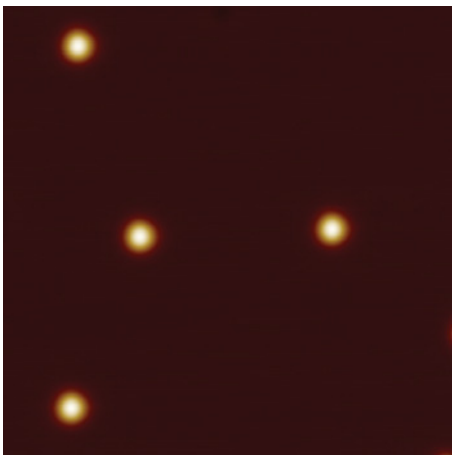

FIG. 1. (Color online) STM topograph of the Li clusters on Cu(100) investigated in the present study. Image size: 18×18 nm^2, $V = 0.8$ V, $I = 0.3$ nA.

B. Scanning tunneling spectroscopy

dI/dV spectra were recorded on the bare Cu surface and on single Li clusters with no other cluster within a radius of at least 10 nm. The stability (position and shape) of the cluster and tip configuration was checked by taking topographs before and after acquisition of the dI/dV spectrum, as well as by repeatedly acquiring dI/dV spectra of the bare Cu surface. The cluster sometimes moved or hopped while ramping the bias voltage but never fragmented. Typical dI/dV spectra together with $z(V)$ curves for the bare substrate and on the center of the Li clusters are presented in Fig. 2.

On the bare Cu(100) surface, a series of resonances is observed (upper spectrum in Fig. 2) that have been previously described as Stark-shifted image-state resonances.[1] Due to the presence of the STM tip and the associated strong electric field, these states are often referred to as FER's. For each peak in the dI/dV spectrum, there exists a corresponding step in the $z(V)$ characteristic. Depending on the tip conditions, four to eight resonances are observed up to a bias of 9 V. The lowest resonance at about 4.8 V is less sensitive to the tip shape and has been considered as a measure for the local work-function variations.[3,4,7] The lower spectra in Fig. 2 were taken on top of a single Li cluster. The spectrum differs strongly from the bare Cu(100) surface. Besides the apparent variations in the peak positions and spacing, also the relative intensities differ from the flat metal surface. Above 7.5 V, the series of resonances on top of the cluster resembles the spectrum on the bare surface, although significantly shifted in energy. The position of the resonances also depends on the tip conditions. On the Li cluster, the lowest, and relatively broad, resonance is located at about 3.3 V followed by a noisy low conductance area at about 4 V. A small and sharp resonance is found at 4.5 V while the former first FER of the bare surface is only faintly observed at 4.8 V. At somewhat below 7 V, the dI/dV spectrum shows a doublet with apparent lower peak intensities and broader linewidth.

To gain more insight into the origin and lateral extension of the FER's, a series of dI/dV spectra was acquired along a line 3 nm long from the center of the Li cluster toward the bare Cu surface (see Fig. 3). Several essential features can be distinguished. New resonances (blue lines in Fig. 3) appear

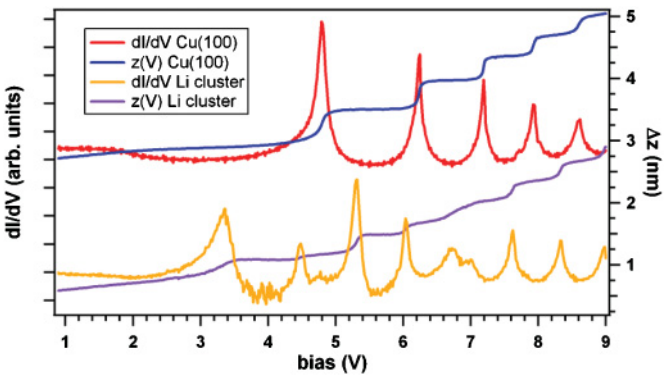

FIG. 2. (Color) dI/dV spectra and corresponding $z(V)$ curves obtained on the bare Cu(100) surface and on the center of the Li cluster in constant current mode. The spectra are shifted for clarity. Set-point parameters are 0.8 V, 0.3 nA.

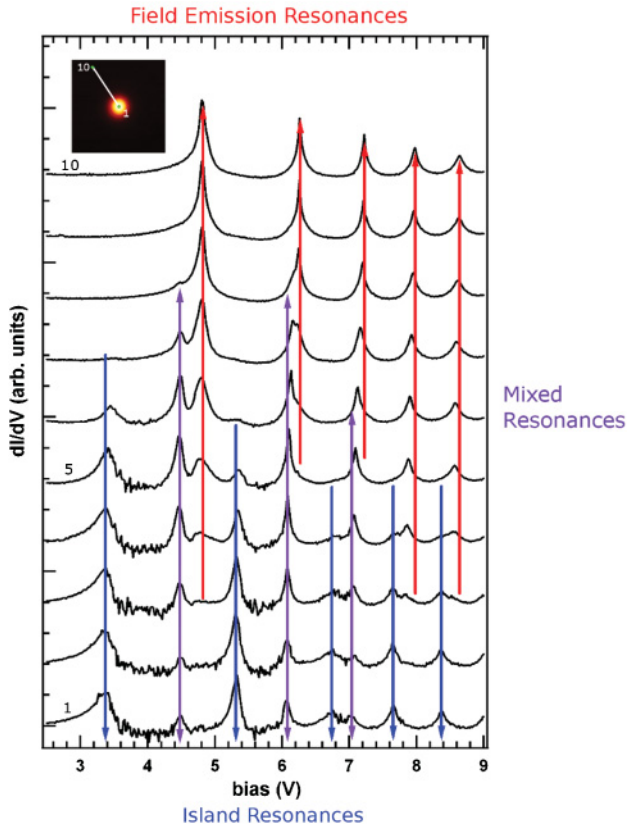

FIG. 3. (Color) dI/dV spectra acquired along a line from the center of the Li cluster (bottom spectrum, labeled 1) to a point of the Cu surface 3 nm away from the cluster (top spectrum, labeled 10). The evolution from island resonances (in blue) and mixed resonances (in purple) localized on the Li cluster to the original FER's delocalized on the Cu(100) metal surface (in red) can be directly followed in this graph when going from spectrum 1 (higher signal from island resonances) to spectrum 10 (higher signal from FER's) through spectrum 5 (higher signal from mix resonances)

separated from the FER's of the pristine Cu(100) surface (red lines). These resonances are most prominent on the top of the cluster and disappear gradually when moving away from it. Therefore, the underlying electronic states are localized on the cluster and will be called island-localized FER's (ILFER's). Below 7.5 V, when approaching the Li cluster, a shoulder develops a few tenths of a volts below the "parent" FER of the pristine Cu(100) (purple lines). This is more clearly seen for the lowest one at 4.5 V. Upon further approaching the cluster, the former shoulder evolves into a narrow well resolved resonance particulary intense at the border of the cluster, as shown in the corresponding dI/dV maps (see Fig. 4). However, the original FER's of the pristine Cu(100) surface loose intensity and eventually vanish when approaching the center of the Li cluster. Above 7.5 V, the larger width of the FER's does not allow to resolve the shoulder peak from the original FER of the pristine Cu(100) surface, but a shift in the peak position indicates the appearance of the shoulder and disappearance of the original FER, meaning that the behavior is similar to that in the lower-energy region. The interpretation of the origin of these resonances is given in the next section, after the description of our theoretical model (see Figs. 9 and 10 below).

The spatial extension of the resonances is best seen in dI/dV maps acquired at the peak positions of the resonances on top of the clusters. The dI/dV maps are presented together with the corresponding STM topographs in Fig. 4. Two main features are observed. There are resonances exhibiting a ring shape at 4.4, 6.04, and 6.98 V (purple lines in Fig. 3), while resonances at 3.34, 5.3, and 6.73 V (blue lines in Fig. 3) are well localized inside the cluster area. The spatial extension is largest for the ring-shaped resonances. These states also show the largest topographical features, which differ strongly for the given bias voltages. It is interesting to note that the rim of the resonances and topographical features is not perfectly circular but rather distorted toward a square structure, in particular for the lower resonances at 3.34 and 4.4 V. The square distortion follows the surface square symmetry. Note that although the tip-sample distance changes significantly in the dI/dV maps (e.g., $\Delta z = 0.4$ nm at 4.4 V), the position of the FER is rather robust, that is, the ring shape is not an artifact of the measurement, and it is confirmed in the model calculations (see the central panel in Fig. 11).

dI/dV maps at the peak positions of the original FER's were also acquired for a single Li cluster and are presented together with their corresponding topographs in Fig. 5. In the topographs, the cluster is imaged with a central depression, i.e., the original FER's are also modified by the presence of the cluster. The dI/dV maps at 4.82 and 6.28 V show an oscillatory ring pattern around the cluster. This pattern is ascribed to the density modulation created by the scattering of FER electrons at the cluster.[12]

Besides the localization of FER's at single Li clusters, we have also studied FER's of closely spaced Li clusters. Some

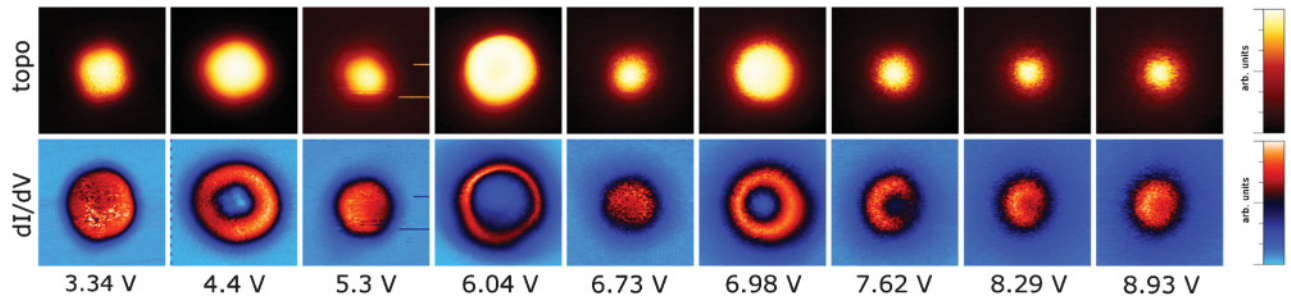

FIG. 4. (Color online) STM topographs and corresponding dI/dV maps of an individual Li cluster acquired at the peak positions of the FER observed in spectrum no. 1 of Fig. 3 taken on top of the cluster. Image size: $4.8 \times 4.8\,\text{nm}^2$.

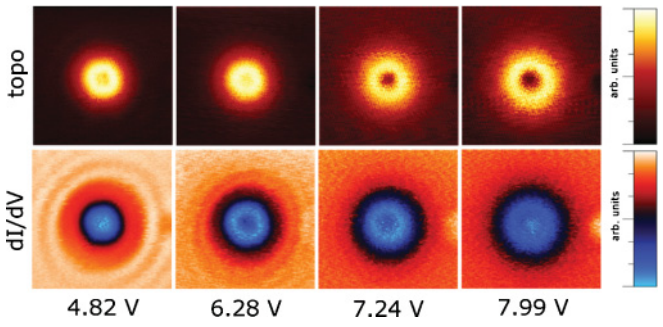

FIG. 5. (Color online) dI/dV maps and topographs of a single Li cluster acquired at the peak positions of the unperturbed FER of the bare Cu(100) surface. Image size: 9×9 nm^2.

examples of dI/dV maps are presented in Fig. 6. We find that if the clusters are closer than the lateral confinement distance of the resonance on the alkali nanoislands, their wave functions start to interact, the difference being particularly significant between ring-shaped resonances and ILFER's (circular patterns). More precisely, the first two dI/dV maps at 4.45 V were acquired for two clusters at a distance of 1.4 and 2.8 nm. The next two were acquired at the same separation 2.8 nm but at two different bias voltage values, 5.3 and 6.02 V, respectively. The last dI/dV map was taken at a somewhat larger separation distance 3.1 nm and 5.91 V. It is clear that this lateral confinement distance is appreciably larger for the two ring-shaped resonances at 4.45 and 6.02 V as compared to the localized ILFER at 5.3 V, regardless of whether or not this latter appears at a higher bias voltage value (5.3 V) than the first one (4.45 V). Therefore, resonances localized on the island (ILFER's) could be seen as "core" states of the cluster, while those at the perimeter can be seen as "valence" states, in the sense that these latter start to interact earlier as the two clusters forming the dimer get closer. This could be already anticipated by looking at the dI/dV maps shown in Fig. 4.

III. THEORETICAL METHODS

The main objective of the present theoretical contribution is to explain the physics behind the experimental observations and to draw some conclusions common to all the alkali ad-island structures deposited on the nobel metal surfaces with a projected band gap that, furthermore, can be applied to other kinds of nanostructures deposited on metal surfaces. We do not seek to achieve full quantitative agreement with the experiment, since a 3D calculation is required to reproduce the measured dI/dV maps. Therefore, we restrict our study to the cylindrically symmetric case with the tip apex positioned right above the center of an alkali island represented within

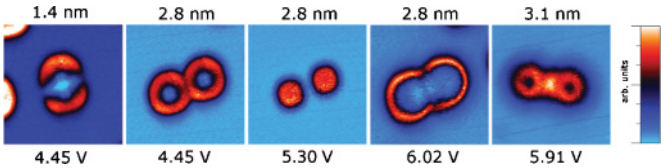

FIG. 6. (Color online) dI/dV maps of Li cluster dimers. The distance between the clusters and the bias voltage is given above and below each image, respectively. Image size: 9×9 nm^2.

the cylindrical jellium model. Such an approach strongly reduces the calculation time and, more importantly, allows an unambiguous assignment of the origin of the different resonant structures appearing within each m-symmetry subspace. Here, m is the projection of the angular momentum on the symmetry axis, z. Moreover, as we will show below, only the $m = 0$ intrinsic cluster resonances have a dominant contribution to the experimentally measured spectra. The values of the parameters that define the cylindrical jellium model in the present case have to be considered as effective values. Thus, strictly speaking, they do not correspond to measurable quantities. For example, a direct comparison between the observed apparent diameter and the local work-function change with the ones used in the jellium model is elusive, as the lack of precise knowledge of the chemical composition mentioned above introduces some uncertainties in the values of these quantities. All in all, we are able to explain the basic trends observed in the experiments with the model system that is described in the following.

For the description of the system, we use the model potential for Na ad-atom islands on Cu(111) developed in Refs. 16 and 15 on the basis of density-functional-theory (DFT) calculations and adapt it to the present case of Cu(100). To take advantage of our previous work, we consider Na instead of Li islands; note that the most important features of the model are independent of the alkali metal species. With the Cu(111) surface represented by an unscreened model potential,[19] the DFT calculations performed in Ref. 16 yield the island-induced one-electron potential defined as $\Delta U = U^{\mathrm{DFT}}_{\mathrm{Na+Cu(111)}} - U^{\mathrm{DFT}}_{\mathrm{Cu(111)}}$. Here $U_{\mathrm{Na+Cu(111)}}$ and $U_{\mathrm{Cu(111)}}$ are the full (Hartree + exchange-correlation) DFT potentials for the Na nanoisland on Cu(111) and bare Cu(111), respectively. We then construct the model one-electron potential U representative for the alkali island on the Cu(100) surface in the presence of the STM tip as

$$U(\rho,z) = \Delta U(\rho,z) + U_{\mathrm{Cu(100)}}(z) + U_{\mathrm{tip}}(V,z) + U_{\mathrm{abs}}(z), \tag{1}$$

where (ρ,φ,z) are the cylindrical coordinates with the z axis perpendicular to the metal surface, going through the center of the island, and corresponding to the axis of the STM tip.

$U_{\mathrm{Cu(100)}}(z)$ is the periodic one-dimensional model potential that reproduces the essential features of the projected band structure of the Cu(100) surface at the $\bar{\Gamma}$ point, including the image states,[19] and the projected band gap from about $+1.6$ to $+7.8$ eV with respect to the Fermi level. This approximately corresponds to -3 to $+3$ eV with respect to the Cu(100) surface vacuum level.

$U_{\mathrm{tip}}(V,z)$ in Eq. (1) is the potential due to the presence of the STM tip, where the dependence on the bias V is explicitly introduced. Since the FER's under study correspond to the high bias case, an electron mainly tunnels not from the last group of atoms at the tip apex but from the mesoscopic surface of the tip. As the lateral extension of the alkali island is typically only 1 nm, the finite radius of curvature of the tip (in the 10-nm range) can be neglected. U_{tip} is then calculated within the flat tip approximation on the basis of well-tested models.[11,12] This allows inclusion of the applied electric field in the tunneling junction and an efficient treatment of the

varying tip-sample distance, mandatory to compare with the STS data taken at high bias voltages. Finally, $U_{\rm abs}$ is the imaginary potential introduced inside the metal to account for the inelastic electron-electron scattering events.[20,21]

Using ΔU obtained for the Cu(111) surface to construct the total potential $U(\rho,z)$ for the present Cu(100) surface case is certainly an approximation; nonetheless, ΔU includes the essential characteristics of the ad-island induced potential: (i) the potential well leading to the ad-island localized electronic states, and (ii) the change of the electrostatic potential above the ad-island surface (often referred to as a local work function). As we will see below, these are the main ingredients allowing us to explain the experimental observations.

Given the potential $U(\rho,z)$, the wave-packet-propagation technique (WPP) has been applied for the calculation of the energy dependence of the electron transmission coefficients across the tunneling barrier. This allows us to obtain the different tunneling characteristics, such as current voltage, conductance voltage, or distance voltage. In addition, the real space maps of the electronic wave function at a given energy, as well as the projected density of electronic states (PDOS), can be obtained, greatly simplifying the assignment of the resonant states in the metal-nanoisland-tip junction. The details of the WPP method can be found elsewhere.[22,23] Here we only give the aspects specific for the present study. In brief, the one-electron wave packet incident from the STM tip is propagated through the junction by solving the time-dependent Schrödinger equation (TDSE). The electronic wave function is represented on a (ρ,z) grid in cylindrical coordinates,

$$\Psi(\rho,\varphi,z,t)=\sum_m \psi_m(\rho,z,t)e^{im\varphi}. \tag{2}$$

For the case of cylindrical symmetry considered here, m is a good quantum number, so that different m subspaces are treated independently. Provided the initial conditions $\psi_m(\rho,z,t=0)$, the time evolution of $\psi_m(\rho,z,t)$ is given by

$$\psi_m(\rho,z,t)=e^{-iH_m t}\psi_m(\rho,z,t=0), \tag{3}$$

with an effective Hamiltonian,

$$H_m=-\frac{1}{2}\frac{\partial^2}{\partial z^2}-\frac{1}{2\rho}\frac{\partial}{\partial\rho}\rho\frac{\partial}{\partial\rho}+\frac{m^2}{2\rho^2}+U(\rho,z). \tag{4}$$

Equation (3) is solved via the short-time propagation with the split-operator technique[24,25] as detailed in Refs. 22 and 23. For a cylindrical tip of radius $R_{\rm tip}$ (typically values $R_{\rm tip}=6$ nm were used in the cylindrical shape simulation box), the electronic states propagating in forward and backward directions are given by

$$\chi_{mj}(\rho,z)=\frac{1}{\sqrt{2\pi}}e^{\pm ikz}J_m\left(\rho X_j^m/R_{\rm tip}\right)e^{im\varphi}, \tag{5}$$

where $J_m(x)$ is the Bessel function of order m and X_j^m is the jth zero of $J_m(x)$ (different from $x=0$ for $|m|\neq 0$). The couple (m,j) therefore defines a given asymptotic channel for electron motion inside the tip. The corresponding energy is given by (the $\pm m$ states are degenerate)

$$E_j^m(k)=\left(X_j^m/R_{\rm tip}\right)^2/2+k^2/2. \tag{6}$$

We then set the initial wave packet incident from the tip onto the junction (in the negative direction of the z axis) as follows:

$$\psi_{mj}(\rho,z,t=0)=\mathrm{e}^{-ik_0z-(z-z_0^2)/\sigma^2}J_m\left(\rho X_j^m/R_{\rm tip}\right), \tag{7}$$

where the parameters k_0 and σ are chosen in such a way that (i) the initial wave packet has no overlap with the STM junction, and (ii) the energy spectrum of the initial wave packet covers the energy range of interest.

The tunneling current is determined by the electron transmission matrix from the tip into the substrate. Because of the absorbing potential introduced inside the Cu(100) metal, the direct calculation of the transmission coefficient from the WPP is, strictly speaking, not possible, as the flux transferred into the Cu(100) is not preserved. We then proceed as follows. With $\psi_{mj}(\rho,z,t=0)$ defined by Eq. (7), the electron-energy resolved reflection matrix of the junction $\mathbb{R}^m_{j'j}(V,E)$ is obtained within each m-symmetry subspace inside the tip via the "virtual detector method"[26] associated to nonreflecting boundary conditions.[27] The $\mathbb{R}^m_{j'j}(V,E)$ matrix element gives the probability for an electron incident within the (m,j) channel to be reflected back into the tip within the (m,j') channel. Here we underline the dependence of the scattering properties of the junction on the bias V. From the flux conservation principle, the total transmitted flux J_j^m is given by the difference between incident and total reflected flux:

$$J_j^m(E,V)=1-\sum_{j'}\mathbb{R}^m_{j'j}(E,V), \tag{8}$$

where the summation runs only over the open channels $E\geqslant(X^m_{j'}/R_{\rm tip})^2/2$. Then, the total tunneling flux through the junction at a given energy E is given by

$$J(E,V)=2\sum_{mj}\left(1-\sum_{j'}\mathbb{R}^m_{j'j}(E,V)\right), \tag{9}$$

where the summation runs only over the open channels, and the factor 2 stands for the spin statistics. From $J(V,E)$ one obtains the total current $I(V)=\int_{E_F}^{E_F+eV}J(E,V)\,dE$, and therefore the current-voltage, conductance-voltage, or distance-voltage characteristics. E_F is the Fermi level of the Cu(100), so that E_F+eV is the tip Fermi level. Note that we do not account for the modification of the alkali island because of the bias field in the junction. Provided $R_{\rm tip}$ is large enough, that is, the spectrum of j states is sufficiently dense, the energy of the different resonant features in the tunneling current converges with respect to $R_{\rm tip}$. A typical calculation mesh comprises 500 knots in the ρ coordinate and 1024 knots in the z coordinate. The typical propagation time is 4000 a.u. covered in 40 000 time steps.

As mentioned in the experimental section, the observed peaks that appear in the differential conductance (dI/dV) point spectra at energies between 3 and 9 eV above the Fermi level correspond to FER's with different character, that is, metal- or islandlike. To identify them in our model calculations, we use the same strategy as in the experiment: compare the point spectra taken on top of the clean metal surface with the spectra on top of the alkali island. For the clean metal surface, the 1D version of the WPP procedure[12] has been used.

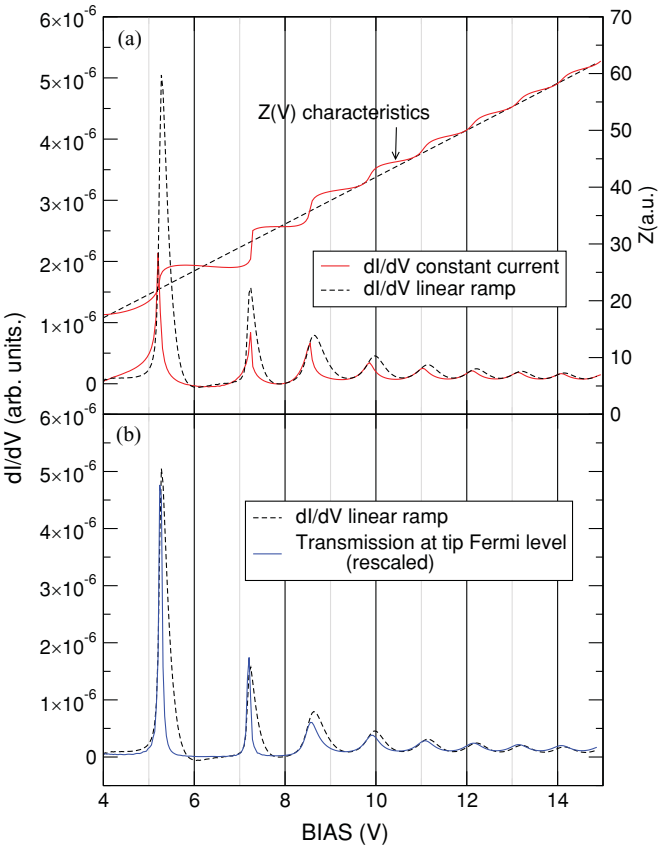

FIG. 7. (Color online) (a) Comparison between constant current and linear $Z(V)$ ramp dI/dV spectra for the Cu(100) surface. (b) Comparison between $dI/dV(V)$ and transmission of the junction at the tip Fermi level for the same linear $Z(V)$ ramp. See text for details.

The calculated constant current distance-voltage characteristic $Z(V)$ shows sharper (energies in the projected band gap) or smoother (energies outside the gap) steps at values V_i that essentially correspond to the different resonance energies $E_i = eV_i$ [see Fig. 7(a)]. To make the computation of the nanoisland dI/dV tractable numerically, we approximate the constant current $Z(V)$ by a linear ramp. The validity of this approximation is assessed in Fig. 7, where we present the calculated tunneling characteristics for the clean Cu(100) surface. A comparison of the corresponding dI/dV curves, shown in Fig. 7(a), permits us to conclude that only minor changes in peak positions with some broadening of the peaks (mostly for resonances in the gap) appear. Indeed, this approximation is not only convenient to speed up the calculations, as there is no need to find the constant current $Z(V)$ characteristic, but it also permits using the same $Z(V)$ to simulate dI/dV curves on top of both the clean metal surface and the alkali island. In this way, it is straightforward to identify the character of resonances simply from the peak positions in the spectra, something that cannot be done so accurately in the experiment due to an artificial energy shift introduced by the constant current dynamic method of data acquisition.

As one would expect [see Fig. 7(b)], the FER's appear equally well in the dI/dV curves and in the total transmission at the tip Fermi level[12] for a given $Z(V)$. In fact, the presence of resonances in the latter is the reason for the appearance of peaks in the corresponding dI/dV spectrum. We thus end up with several possible ways of doing the resonance analysis: (i) dI/dV curves; (ii) m-resolved transmission at the tip Fermi level: $\mathbb{T}^m(E_F+eV,V) = \sum_j [1 - \sum_{j'} \mathbb{R}^m_{j'j}(E_F+eV,V)]$; (iii) m- and energy-resolved transmission for the given fixed bias V, and tip-sample distance Z: $\mathbb{T}^m(E,V) = \sum_j [1 - \sum_{j'} \mathbb{R}^m_{j'j}(E,V)]$; and (iv) PDOS analysis where the resonances (quasistationary states) of the junction appear as Lorentzian peaks in the energy dependence of PDOS for the given V, Z parameters. Approaches (i) and (ii) are linked with the dynamical experimental method, where changing the bias (the energy at which the electronic states of the junction are probed) introduces the energy shift of these very states. Approaches (iii) and (iv) are aimed at finding all existing resonance states for the given experimental condition, that is, for the given potential of the junction. Observe that, strictly speaking, the quasistationary states are the decaying solutions for the given Hamiltonian, and, therefore, they are rigorously defined only in these last two cases.

As far as the resonance assignment is concerned, the symmetry considerations appear particularly handy in the present case. The metal-like resonances are delocalized along the surface and have contributions from all m channels, while the (cylindrical) island-localized resonances have well-defined m character. It is worth noting that because of the $m^2/2\rho^2$ centrifugal barrier, the number of island-localized states decreases with increasing m and their energy rises.[16] The transmission through the island is then fully determined by a limited number of m channels (in practice, $m = 0, \pm 1, \pm 2$), as shown in Fig. 9 (see below).

In Fig. 8, we show the energy and bias voltage dependence of the density of states PDOS(E,V) along a given linear $Z(V)$ characteristic for the $m = 0$ symmetry subspace. The three panels (a), (b), and (c) correspond to the clean metal Cu(100) surface, the case of $d = 1.07$ and 1.77 nm alkali nanoislands deposited on Cu(100), respectively, where d is the diameter of the island. The energy position and the widths of the peaks in PDOS(E,V) reflect the energies and widths of the underlying quasistationary states, which are independent of the choice of the initial state used in the WPP for the PDOS calculation. The intensity of the peaks, on the other hand, is given by the overlap between the resonance wave function and the initial state used in the WPP.[23]

A simple comparison between the clean surface [panel (a)] and ad-island results [panels (b) and (c)] allows one to assign the different resonances (in particular, to reveal the island-localized states) and their evolution upon the change of the experimental conditions. Thus, the additional bright lines that appear in the calculated PDOS(E,V) for the island on top of the metal surface [panels (b) and (c)] correspond to island-induced states whose energies are not very close to the other FER's, as compared to their width. These well-resolved sharp resonances are then located approximately between -3 and $+3$ eV with respect to the Cu(100) surface vacuum level [$+1.6$ and $+7.8$ eV above the Cu(100) Fermi level], that is, in the projected band gap at $\bar{\Gamma}$. As the energy is raised above the projected band gap, the lifetimes of the resonances are appreciably reduced because of the efficient decay via an

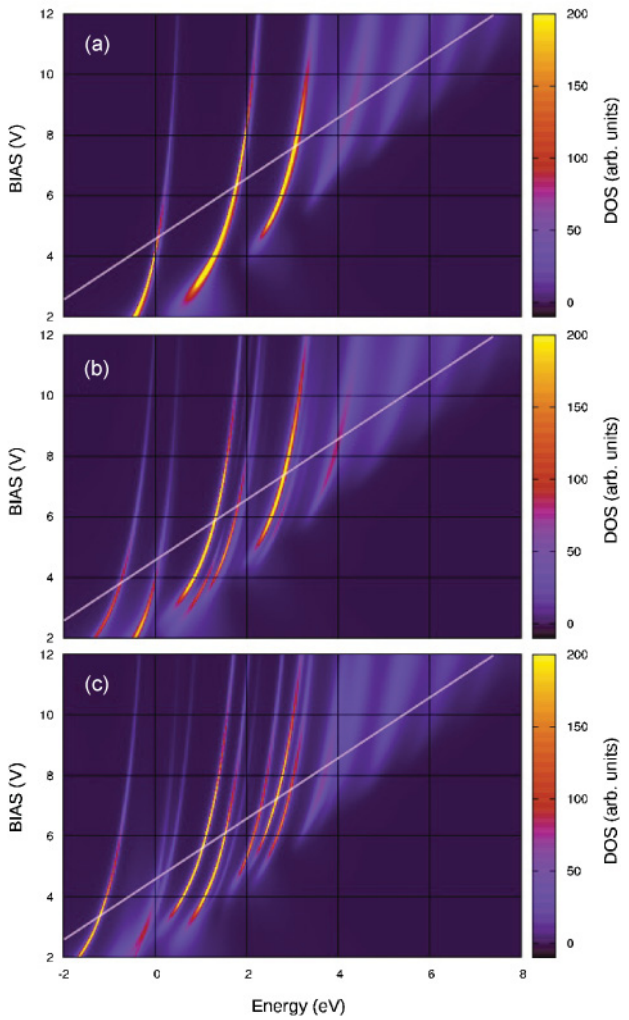

FIG. 8. (Color online) Contour plots of the energy E and bias voltage V dependence of the $m = 0$ component of the density of states PDOS(E,V) for the clean Cu(100) metal surface (a), and two alkali islands characterized by different diameter $d = 1.07$ nm (b) and $d = 1.77$ nm (c). The energy is measured with respect to the vacuum level of the Cu(100) surface. The use of the same linear $Z(V)$ characteristic in both cases permits a direct identification of the first islandlike resonances as additional lines to the clean metal FER's. The white oblique straight lines are defined by the linear $E(V) = eV - W$ relation, where W is the Cu(100) work function (4.6 eV).

electron escape into the metal. Only broad overlapping features are then observed in agreement with experimental data.

Before entering a detailed discussion that includes the assignment of the different resonant states, let us first present some basic considerations relying on the general properties of nanosized alkali ad-islands. Indeed, the complex resonance pattern observed in this study calls for a guiding line allowing one to have a better understanding of the data. As follows from previous works,[15,16] in the absence of the STM tip the attractive potential associated with the alkali ad-island is sufficiently strong to lead to a series of island-induced quasistationary electronic states. The finite lifetime of these states is due to the coupling with the substrate, which enables population decay. The lowest-energy resonances are well localized inside the island and correspond to the quantum-well state (QWS's) of the complete alkali overlayer quantized by the island boundaries. Within the $m = 0$ symmetry, each following ℓ state develops an additional zero in the wave-function structure along the island in the ρ direction. Because of their large binding energies, the QWS's do not appear in the energy range relevant for the present study of the FER's. In addition to the QWS's, the image-potential-like (IS's) states localized in front of the island were reported.[16] The lowest n IS's are pinned to the local vacuum level in front of the island. Here n is the quantum number of the IS linked with the nodal structure perpendicular to the island surface. As n grows, an electron moves far enough from the island to "probe" the finite size of the latter and the finite range of the associated attractive dipole. The high n states then merge into the series of the IS's of the substrate. As for the QWS's, for fixed symmetry and quantum number n a series of states is formed. Each next state develops an additional zero in the ρ direction because of the quantization by reflection at island boundaries. Thus, the image-potential-like states localized in front of the island are characterized by the two (n and ℓ) quantum numbers. n corresponds to the quantization of the electron motion perpendicular to the surface in the z direction, similarly to the conventional IS's of the pristine metal surface, while ℓ reflects the nodal structure in the ρ direction parallel to the surface. Importantly, the lifetime of the resonances with given n rapidly decreases with increasing energy (ℓ quantum number). This is linked with an energy dependence of the electron escape through the island boundaries,[13–16] and it also explains why only a limited number of states could be observed.

When the bias is applied to the STM junction, the corresponding electric field overrides the image potential so that the IS's evolve into the states of the linear ramp potential, that is, FER's. They can be considered as Stark-shifted IS's. We thus expect several types of resonances to be formed in the present system within each m-symmetry subspace.

(i) The modified FER's of the pristine Cu(100) surface with energies equal to that of the island-free case, and wave-function structure in the ρ direction modified by the scattering at the island boundaries. Since these states are delocalized along the surface, they form a 2D continuum characterized by the quantum number n and parabolic energy dispersion $E_n(V,k_{||}) = E_n(V) + k_{||}^2/2m^*$. $E_n(V)$ is the energy of the FER at $\bar{\Gamma}$, and $k_{||}$ is the electron momentum parallel to the surface. Within the model potential for Cu(100) (Ref. 19) that we use, the effective mass is $m^* = 1$.

(ii) Nondispersing FER's bound by the attractive potential well in front of the island and evolving from the island localized IS's. These states are characterized by the two quantum numbers n and ℓ reflecting the nodal structure perpendicular and parallel to the island surface, respectively. By analogy with island-localized image states, one can expect that the energies of the island-localized FER's can be approximated by[16]

$$E_{n\ell}^m(V) = E_n(V) + \left(X_\ell^m/R\right)^2/2, \qquad (10)$$

where R is the radius of the island and X_ℓ^m is the zero of the corresponding Bessel function. $E_n(V)$ accounts for the local change of the work function above the island, and the second term corresponds to the quantization by scattering at

island boundaries. It is noteworthy that for a large enough island radius ($R \to \infty$), $E_n(V)$ converges to the $\bar{\Gamma}$ energies of the FER's of the Cu(100) surface with a complete alkali overlayer.

(iii) Finally, the attractive potential of the alkali island should lead to the localization of the 2D Cu(100) FER's. Similar to the surface state or image-state localization by an attractive adatom potential,[28–31] we expect the nondispersive component of these resonances to appear below the bottom of the 2D continuum for each split Cu(100) FER. When close in energy, states (ii) and (iii) can experience an avoided crossing with mixing of their character.

We are now in a position to assign the character of the different resonant structures appearing in Fig. 8. We will focus on the large alkali nanoislands [panel (c)] for which the energy position of the different resonances matches rather well the observed ones. The radial size of the ad-island is an important parameter since, as follows from Eq. (10), it determines the characteristic energy scale for the ρ quantization, that is, the energy separation and the number of the island-localized FER's characterized by the same quantum number n and varying ℓ.

To directly connect between the calculated data and the experimentally measured dI/dV spectra, we show in Fig. 9 the m-resolved transmission at the tip Fermi level: $\mathbb{T}^m(E_F + eV, V) = \sum_j [1 - \sum_{j'} \mathbb{R}^m_{j'j}(E_F + eV, V)]$ for the $m = 0$ and 1 symmetry subspaces. The results for the clean Cu(100) surface are compared with the alkali nanoisland case along the same distance-voltage characteristic $Z(V)$. Basically, the peak positions reported in Fig. 9 correspond to the cut of the 2D plots of the energy and bias voltage dependence of the PDOS (Fig. 8) along the straight lines shown in white in Fig. 8.

Consistent with the delocalized character of the FER's of the Cu(100) surface, their energies at $\bar{\Gamma}$ are independent of m (see the gray vertical lines in Fig. 9). We label these resonances as FER$_n$ according to their quantum number ($n = 1,2,\ldots$). Because of the flat tip approximation and the same distance-voltage characteristic $Z(V)$ used both for the clean surface and ad-island, the FER's of the Cu(100) surface are also present in the ad-island case. They correspond to the electron tunneling from the tip into the surface area outside the alkali island, and provide a good reference for observation of the island-specific features. The emergence of the island-localized states is particularly apparent within the 2–8 V bias range when the resonances fall into the projected band gap of Cu(100) and thus possess a long lifetime, that is, they are sharp and well-resolved. For higher bias, only broad structures can be observed because of the strong coupling with projected bulk bands.[32] The island-induced resonances are labeled according to their n (principal) and ℓ (radial) quantum numbers, where the assignment of the states is explained below.

The calculated transmission curves allow us to draw an important conclusion: not all the resonances will contribute to the experimentally observed signal. As far as the island states are concerned, the transmission is significant for the $m = 0$ subspace only. An electron in this case tunnels from the tip into the surface along the surface normal going through the center of the ad-island, that is, along the lowest potential energy path. For $|m| = 1$, the centrifugal barrier prevents the electrons from approaching the quantization z axis. The overall decrease of $\mathbb{T}^m(E_F + eV, V)$ with increasing m is even more pronounced for $|m| \geqslant 2$ subspaces (not shown). The $m = 0$ resonances will then mainly determine the tunneling current. Furthermore, within the $m = 0$ subspace, several island-localized states dominate the $\mathbb{T}^m(E_F + eV, V)$ and, in this way, they should give the highest contrast in the experimental dI/dV maps. These are the ($n,\ell = 1$) resonances located at 3.4, 5.7, and 7.3 V below the corresponding FER$_n$ of the pristine Cu(100) surface. They are identified with the observed resonances at 3.3, 5.3, and 6.7 V (see Figs. 4 and 5).

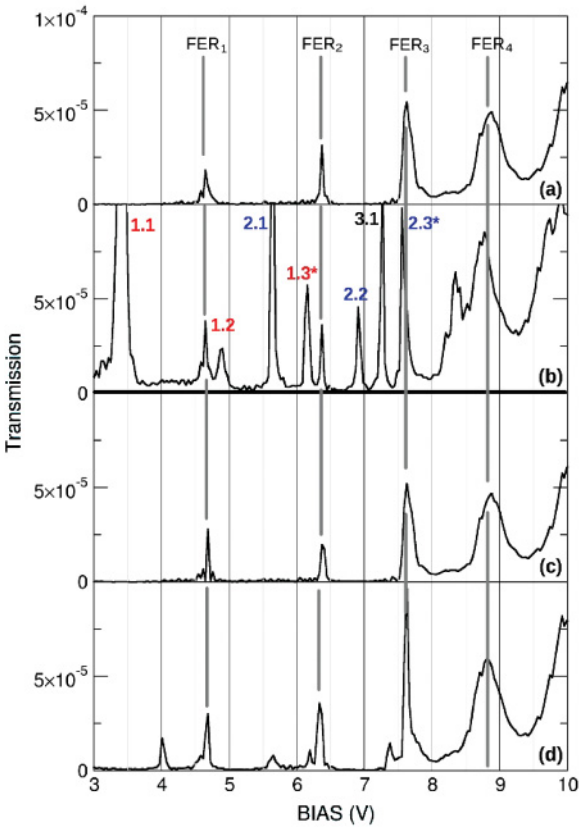

FIG. 9. (Color online) Calculated bias voltage dependence of the transmission at the tip Fermi level $\mathbb{T}^m(E_F + eV, V)$ decomposed in its $m = 0$ [panels (a) and (b)] and $m = 1$ [panels (c) and (d)] components. Results for $d = 1.77$ nm diameter alkali island on Cu(100) [panels (b) and (d)] are presented together with results obtained for the pristine Cu(100) surface [panels (a) and (c)]. The island resonances are labeled using the (n,ℓ) quantum numbers that refer to the number of nodes in the wave function along the perpendicular z axis or the radial ρ axis.

The (n,ℓ) assignment of the resonant structures is done based on the spatial distribution of the corresponding electronic wave functions $\xi^m_{n\ell}$ extracted from the WPP and shown in Fig. 10. The panels of Fig. 10 represent the one-electron charge density $|\xi^m_{n\ell}|^2$ in cylindrical (ρ,z) coordinates with the z axis pointing from the Cu(100) surface into the STM tip. The tip corresponds to a region with a high density parallel to the ρ axis at the top of each panel. The large probability of the electron presence inside the tip results from the choice of the initial conditions with electrons incident at the junction from the flat tip. Observe also the tip retraction for higher-energy states. The oscillatory structure of the wave functions inside

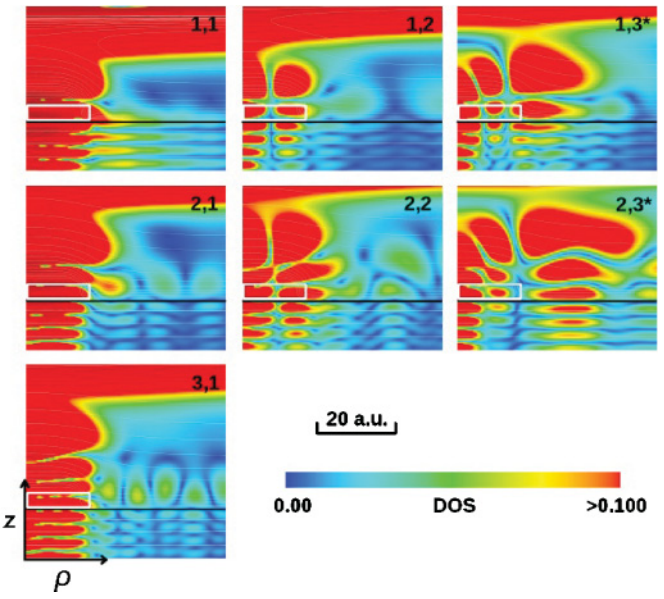

FIG. 10. (Color online) Two-dimensional plots of the electronic density of the island-localized FER's for 1.77-nm-diameter alkali island on Cu(100). Results are presented as a function of the z and ρ cylindrical coordinates. The color code is explained in the inset. The labeling of resonances according to their n, ℓ quantum numbers is the same as in Fig. 9. The z axis runs from the Cu(100) surface (negative z) into the tip (positive z). The thin horizontal line gives the position of the Cu(100) image plane. The cluster is schematically sketched by the white rectangle.

Cu(100) reflects the periodicity of the Cu(100) planes in the z direction. The states presented in Fig. 10 have their energies in the projected band gap of the substrate. The electron density is then exponentially damped into the metal, i.e., an electron propagation along the surface normal is impossible.

The island-induced FER's appear confined to the island area both in the ρ and z directions in the vacuum side between the island and the tip. The overlap between the electronic densities of the island-localized state and the tip reflects the strength of the island-tip coupling and thus the transmission (tunneling current). As discussed above, the n and ℓ quantum numbers define the nodal structure of the island-localized states in the z direction above the island and in the ρ direction along the island, respectively. Thus, the lowest energy transmission resonance (1,1) at 3.4 eV as it appears within the $m = 0$ subspace in Fig. 9 shows no nodes in ρ and a node in z at the island surface. A comparison with the wave functions of the nanosized alkali island-localized image states[16] allows an assignment as the ($n = 1$, $\ell = 1$) ILFER that develops from the ($n = 1$, $\ell = 1$) island-localized image state. The states with additional nodes appearing in the z direction between the tip and the island and no nodes in ρ can be assigned as ($n = 2$, $\ell = 1$) (one additional node) and ($n = 3$, $\ell = 1$) (two additional nodes) ILFER's. Increasing n is associated with the spread of the electronic density farther into the vacuum as far as z behavior is concerned. We observe that the radial shape is very similar for this group of states. The states characterized by additional nodes in the radial direction can be assigned as ($n = 1$, $\ell = 2$) and ($n = 2$, $\ell = 2$) ILFER's depending on the nodal structure in z. Thus, when far in energy from the FER's of the Cu(100) surface, the alkali-island-induced states indeed reflect the confinement properties reported in Ref. 16 with energies following the trends given by Eq. (10). The $\ell = 1$ states give the most prominent transmission resonances because of their nodeless structure along the surface of the island that favors the coupling with the tip, as clearly seen in the corresponding panels of Fig. 10. The $n = 1,2,3$, $\ell = 1$ resonances have energies below the FER's of the Cu(100) surface characterized by the same n. This energy downshift results from the attractive potential of the alkali nanoisland that can be seen as a local reduction of the work function of the surface. The higher the quantum number n of the ILFER, the larger are the distances from the island surface "probed" by an electron. Then, the local effect decreases and the energies of the ILFER approach those of the Cu(100) FER's.

While ($n = 1,2,3$, $\ell = 1,2$) states are well confined in the radial ρ direction to the area of the island, the ($n = 1$, $\ell = 3^*$) and ($n = 2$, $\ell = 3^*$) resonances show quite different spatial extension in the ρ coordinate. The electron density spreads along the surface well outside the island area. Moreover, while the inner part within the island area shows the same z dependence as $\ell = 1$ and 2 resonances, the outer ρ lobe of the wave function has essentially larger extension into the vacuum favoring the coupling with an STM tip. The $\ell = 3^*$ states give then the second highest contribution to the transmission after the $\ell = 1$ resonances. We attribute this particular shape of the $\ell = 3^*$ ILFER's to their origin as the mixed states resulting from the coupling between (i) the islandlike (n, $\ell = 3$) states of the given ℓ series defined by the principal quantum number n and (ii) the 2D localized state split from the FER_{n+1} of the Cu(100) surface.

As we have discussed earlier in this section, the FER's of the Cu(100) surface correspond to the 2D continuum of electronic states propagating along the surface and confined in the direction perpendicular to the surface. According to Simon's theorem,[33] any attractive potential in 2D has a bound state. This is exactly the case of the alkali ad-island since it creates an attractive potential well. Then one might expect to have a bound state below each 2D FER_n continuum with a z dependence of the electron wave function being the same as that of the parent FER_n state, but localized in ρ. The 2D localization by adatoms has been reported for the surface states as well as for the image-potential states.[28–31] A similar effect has been observed in the splitting of bands when an attractive periodic potential with hexagonal symmetry perturbs the originally quasi-free-electron-like bands in rippled graphene[34] or in optical lattices trapping cold atoms.[35] The radial extension of the 2D localized states depends on their energy with respect to the bottom of the corresponding parent continuum, and usually it is quite large. In Fig. 9, one observes that at $\bar{\Gamma}$ the (n, $\ell = 3^*$) transmission resonances are located just below the FER_{n+1} of the pristine Cu(100) surface, that is, exactly in the energy region where one would expect the existence of the 2D localized state split from the FER_{n+1} continuum. Thus, the (n,$\ell = 3$) FER of the "pure" island nature corresponding to the ℓ series given by Eq. (10) and confined to the island will mix with the 2D localized FER_{n+1} of Cu(100), with a larger ρ extension. We use the star in labeling the issuing resonances to underline their "mixed" nature as compared to

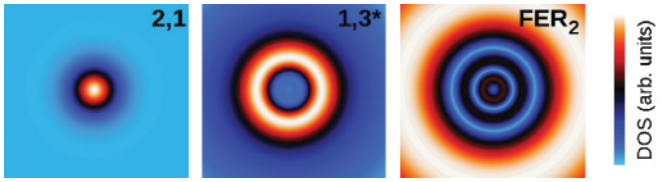

FIG. 11. (Color online) Two-dimensional (x,y) cuts in a plane parallel to the surface at about half-way between the tip and the sample of the full three-dimensional charge densities at three representative selected bias voltage values ($V = 5.7$, 6.1 and 6.4 V) corresponding to an islandlike ($n = 2$, $\ell = 1$), mix ($n = 1$, $\ell = 3^*$), and metal-like resonances (FER_2), respectively.

the "pure" island states. The mixing between the states would also explain the particular shape of the z dependence with electron density more spread into the vacuum outside the island area and reflecting that of the 2D localized FER_{n+1}. Indeed, since the energy of the Cu(100) FER_{n+1} is higher than $E_n^{m=0}(V)$ of the "pure" island series [see Eq. (10)], it is more extended in z. Observe that for this reason the coupling between the STM tip and the $(n,\ \ell = 3^*)$ states is strongest not at the center of the island, but at the ring surrounding the island.

In Fig. 11, we show the two-dimensional (x,y) cuts of the charge density in a plane parallel to the surface at z corresponding to about half-distance between the tip and the sample. The three panels correspond to the bias voltage values at which the islandlike $(n = 2,\ell = 1)$, mix $(n = 1,\ell = 3^*)$, and metal-like FER_2 resonances are observed within the $m = 0$ subspace in Fig. 9. Provided that the dominant contribution to the transmission comes from the $m = 0$ symmetry, the calculated results can be compared with experimentally measured dI/dV maps (see Figs. 4 and 5) revealing striking resemblance. It should be understood, however, that there are essential differences between measured dI/dV maps and simulated charge densities: (i) the m character of intrinsic island resonances is not resolved in the experiments; (ii) the measured dI/dV maps correspond to constant current scans, while the calculated wave patterns simply show the real-space charge distribution of the resonances; (iii) the simulations were performed with $Z(V)$ characteristic obtained for the pristine Cu(100) surface, therefore they neglect the possible change in $Z(V)$ because of the presence of the island; finally (iv) the constant current mode of measurement introduces a rapid variation of the tip sample distance Z at the critical voltage values V_n for resonances with energy $E_n = eV_n$ in the projected gap seen as steps in the $Z(V)$ characteristic, contrary to the constant field case of the linear $Z(V)$ ramp used in the model calculations.

Keeping in mind the words of caution above, the calculated results closely match the experimental observations. Consistent with Fig. 10, the island-induced $(n = 2,\ell = 1)$ resonance appears as a bright spot confined in the island area. It is followed by the mixed $(n = 1,\ell = 3^*)$ resonance appearing as a bright ring surrounding the island and extending outside its area. Finally, for the metal-like FER_2 resonance of the Cu(100) surface, the electrons are repelled from the island area because of the orthogonality constraint with respect to the island-localized states including the mix resonance. The island then appears as depletion, which is fully confirmed by the experiment.

IV. SUMMARY

We have presented a low-temperature scanning tunneling spectroscopy study of FER's of alkali metal clusters on Cu(100). Isolated clusters present a complex FER spectrum composed of localized resonances intrinsic to the clusters together with resonances arising from 2D localization of the substrate FER's around the clusters, which can mix with each other if sufficiently close in energy. Two-dimensional dI/dV maps reveal the spatial extension of the different type of FER's, showing that clusterlike FER's are localized at the center of the alkali islands, whereas substrate-related FER's form ring-shaped structures at the island boundaries. dI/dV maps taken on cluster dimers show that localized FER hybridization occurs for dimers formed by two nearby clusters as long as the separation distance is short enough. This distance depends on the kind of resonance (mixed or ILFER), being shorter for ILFER's as compared to mix resonances.

Based on the comparison between experimental data and results of model calculation, we can formulate the following general rule: starting from the lowest $(n = 1,\ell = 1)$ resonance, the island-induced resonances of islandlike $(n,\ell = 1)$ character give the main peaks in the transmission and experimental dI/dV spectra at the energies comprised between FER_{n-1} and FER_n of Cu(100). The corresponding dI/dV maps show bright spots spatially confined to the island area. Further prominent peaks in the transmission alternating with $(n,\ell = 1)$ ones correspond to the mixed resonances originating from the composition of (n,ℓ) series of the island-localized image states (here $\ell = 3^*$) and 2D-localized state split from the FER_{n+1} of the pristine Cu(100) surface. The corresponding dI/dV maps at resonance energies are expected to show a bright ring surrounding the island and extending outside its area. This theoretical prediction is consistent with our experimental data for bias voltages within the projected band gap of Cu(100). The states observed outside this bias voltage range are so broadened by the coupling with Cu(100) bulk bands that a clear-cut definition of their character is no longer possible. Along the same lines, recent work of Schouteden and Van Haesendonck[36] addressed the island-induced resonances for large Co islands on Au(111). The large width of the resonances above the top of the projected band gap (+3.6 eV with respect to the Fermi level) precludes observation of the split-off states so that only pure islandlike resonances [the $(n,\ell = 1)$ series] and field emission resonances (the FER_n series) of the Au(111) surface could be observed.

How robust are the present results and how representative are the calculations performed for Na nanoislands to interpret the experimental case of Li nanoislands? To answer this question, let us list the most important ingredients of the present theoretical explanation of the experimental data.

(i) The island-localized FER's form a series that can be seen as a quantization of the FER's of the complete alkali overlayer by the island boundaries. For the cylindrical island structure, these states are characterized by the magnetic

quantum number m, vertical (principal) quantum number n, and radial quantum number ℓ as given by Eq. (10).

(ii) Because of the centrifugal barrier, $m = 0$ states give a dominant contribution to the transmission and thus to the tunneling current.

(iii) The alkali nanoisland creates an attractive potential well. As a result, for fixed quantum number n, the $E_{n\ell}^{m=0}(V)$ series of the island-localized states starts with $\ell = 1$ well below the FER_n continuum of the substrate metal surface.

(iv) The attractive potential well due to the alkali nanoisland leads to the 2D localization of the FER's of the substrate metal surface. Thus, the 2D localized state is formed below the bottom of the corresponding continuum of the "parent" FER_n at $\bar{\Gamma}$. Contrary to the "pure" islandlike states, the 2D localized FER's have spatial extension along the surface that is essentially larger than the island area.

(v) When close in energy, the islandlike states ($n,\ell \geqslant 2$) hybridize with 2D localized FER's with principal quantum number $n' > n$ leading to the formation of mixed states.

(vi) Because of their spatial extension, the islandlike ($n,\ell = 1$) states and the mix states give the main contribution to the tunneling current.

(vii) Consistent with electronic density profiles, the islandlike ($n,\ell = 1$) states are predicted to appear in dI/dV maps as bright spots confined to the island area. The mixed states should appear as a ring structures extending outside the island in the direction parallel to the surface.

(viii) The different character of resonances is well resolved only for the bias values such that the states fall into the projected band gap of the substrate. Outside this range, the structures are too broad because of the fast electron escape into the bulk metal.

The points listed above are not specific for a given 2D nanostructure and substrate. Their common underpinning is the fact that the work function of the nanostructure is lower than the work function of the substrate so that it creates an attractive potential well. Thus, the present theoretical conclusions are robust and not specific for the Cu(100) substrate and Na nanoislands modeled within the free-electron (jellium) approximation as here. We argue that similar results should be obtained for a variety of ad-island–substrate systems (including periodic arrays) whenever the spatial variations of the work function (substrate and adsorbate) are sufficiently large, and when the substrate possesses a band gap in the surface-projected electronic structure that contains the vacuum level, allowing for the series of FER's to be resolved.

ACKNOWLEDGMENTS

We acknowledge partial financial support from the European Research Council (StG 203239), the Spanish Ministerio de Ciencia e Innovación (MAT2010-15659 and FIS2010-19609-C02-01), the Basque Government-University of the Basque Country G.V.-UPV/EHU (IT-366-07), and the Catalan Agència de Gestió d'Ajuts Universitaris i de Recerca (2009 SGR 695). A.M. acknowledges the spanish Ministerio de Ciencia e Innovacion for financial support through the RyC program.

[1] G. Binnig, K. H. Frank, H. Fuchs, N. Garcia, B. Reihl, H. Rohrer, F. Salvan, and A. R. Williams, Phys. Rev. Lett. **55**, 991 (1985); R. S. Becker, J. A. Golovchenko, and B. S. Swartzentruber, *ibid.* **55**, 987 (1985).

[2] J. A. Kubby, Y. R. Wang, and W. J. Greene, Phys. Rev. Lett. **65**, 2165 (1990).

[3] T. Jung, Y. W. Mo, and F. J. Himpsel, Phys. Rev. Lett. **74**, 1641 (1995).

[4] M. Pivetta, F. Patthey, M. Stengel, A. Baldereschi, and W.-D. Schneider, Phys. Rev. B **72**, 115404 (2005).

[5] H.-C. Ploigt, C. Brun, M. Pivetta, F. Patthey, and W.-D. Schneider, Phys. Rev. B **76**, 195404 (2007).

[6] C. L. Lin, S. M. Lu, W. B. Su, H. T. Shih, B. F. Wu, Y. D. Yao, C. S. Chang, and T. T. Tsong, Phys. Rev. Lett. **99**, 216103 (2007).

[7] P. Ruffieux, K. Aït-Mansour, A. Bendounan, R. Fasel, L. Patthey, P. Gröning, and O. Gröning, Phys. Rev. Lett. **102**, 086807 (2009).

[8] J. Li, W. D. Schneider, R. Berndt, and S. Crampin, Phys. Rev. Lett. **80**, 3332 (1998).

[9] J. Lagoute, X. Liu, and S. Fölsch, Phys. Rev. Lett. **95**, 136801 (2005).

[10] M. Feng, J. Zhao, and H. Petek, Science **320**, 359 (2008).

[11] J. M. Pitarke, F. Flores, and P. M. Echenique, Surf. Sci. **234**, 1 (1990).

[12] J. I. Pascual, C. Corriol, G. Ceballos, I. Aldazabal, H.-P. Rust, K. Horn, J. M. Pitarke, P. M. Echenique, and A. Arnau, Phys. Rev. B **75**, 165326 (2007).

[13] S. Crampin, H. Jensen, J. Kröger, L. Limot, and R. Berndt, Phys. Rev. B **72**, 035443 (2005).

[14] J. Kröger, L. Limot, H. Jensen, R. Berndt, S. Crampin, and E. Pehlke, Prog. Surf. Sci. **80**, 26 (2005).

[15] T. Hakala, M. J. Puska, A. G. Borisov, V. M. Silkin, N. Zabala, and E. V. Chulkov, Phys. Rev. B **75**, 165419 (2007).

[16] A. G. Borisov, T. Hakala, M. J. Puska, V. M. Silkin, N. Zabala, E. V. Chulkov, and P. M. Echenique, Phys. Rev. B **76**, 121402(R) (2007).

[17] R. D. Diehl and R. McGrath, Surf. Sci. Rep. **23**, 43 (1996).

[18] I. Ohsaki and T. Oguchi, Surf. Sci. **438**, 26 (1999).

[19] E. V. Chulkov, V. M. Silkin, and P. M. Echenique, Surf. Sci. **437**, 330 (1999).

[20] J. B. Pendry, *Low Energy Electron Diffraction* (Academic, London, 1974).

[21] R. García, J. J. Sáenz, J. M. Soler, and N. García, Surf. Sci. **181**, 69 (1987).

[22] A. G. Borisov, A. K. Kazansky, and J. P. Gauyacq, Phys. Rev. Lett. **80**, 1996 (1998); Phys. Rev. B **59**, 10935 (1999); Surf. Sci. **430**, 165 (1999).

[23] E. V. Chulkov, A. G. Borisov, J. P. Gauyacq, D. Sánchez-Portal, V. M. Silkin, V. P. Zhukov, and P. M. Echenique, Chem. Rev. **106**, 4160 (2006).

[24] M. D. Feit, J. A. Fleck Jr., and A. Steiger, J. Comput. Phys. **47**, 412 (1982).

[25] C. Leforestier, R. H. Bisseling, C. Cerjan, M. D. Feit, R. Friesner, A. Guldberg, A. Hammerich, G. Jolicard, W. Karrlein, H. D. Meyer, N. Lipkin, O. Roncero, and R. Kosloff, J. Comput. Phys. **94**, 59 (1991).

[26]J. Sjakste, A. G. Borisov, J. P. Gauyacq, and A. K. Kazansky, J. Phys. B **37**, 1593 (2004).
[27]D. Kosloff and R. Kosloff, J. Comput. Phys. **52**, 35 (1983).
[28]F. E. Olsson, M. Persson, A. G. Borisov, J.-P. Gauyacq, J. Lagoute, and S. Fölsch, Phys. Rev. Lett. **93**, 206803 (2004).
[29]L. Limot, E. Pehlke, J. Kröger, and R. Berndt, Phys. Rev. Lett. **94**, 036805 (2005).
[30]V. S. Stepanyuk, A. N. Klavsyuk, L. Niebergall, and P. Bruno, Phys. Rev. B **72**, 153407 (2005).
[31]A. G. Borisov, A. K. Kazansky, and J. P. Gauyacq, Phys. Rev. B **65**, 205414 (2002).
[32]C. Corriol, V. M. Silkin, D. Sánchez-Portal, A. Arnau, E. V. Chulkov, P. M. Echenique, T. von Hofe, J. Kliewer, J. Kröger, and R. Berndt, Phys. Rev. Lett. **95**, 176802 (2005).
[33]B. Simon, Ann. Phys. (NY) **97**, 279 (1976).
[34]B. Borca, S. Barja, M. Garnica, D. Sánchez-Portal, V. M. Silkin, E. V. Chulkov, C. F. Hermanns, J. J. Hinarejos, A. L. Vázquez de Parga, A. Arnau, P. M. Echenique, and R. Miranda, Phys. Rev. Lett. **105**, 036804 (2010).
[35]B. Wunsch, F. Guinea, and F. Sols, New J. Phys. **10**, 103027 (2008).
[36]K. Schouteden and C. Van Haesendonck, Phys. Rev. Lett. **103**, 266805 (2009).